# KINETICS AND MECHANISM OF THE SILVER (I) OXIDE TO SILVER (II) OXIDE LAYER ELECTROOXIDATION REACTION

R. C. Salvarezza, J. Gómez Becerra and A. J. Arvia

Instituto de Investigaciones Fisicoquímicas Teóricas y Aplicadas (INIFTA), Facultad de Ciencias Exactas, Universidad Nacional de La Plata, Sucursal 4, Casilla de Correo 16, (1900) La Plata, Argentina

**Abstract**—The electroformation of Ag(II) oxide layer during the anodization of silver in 0.1 M NaOH is investigated under potentiostatic and potentiodynamic conditions. Results are discussed in terms of nucleation and growth models and statistical analysis of induction times related to the nucleation kinetics of Ag(II) oxide crystals. The best fitting of results comes out from the application of a progressive nucleation and 3-D growth model under mass transfer control where diffusion of species from the electrode to growing sites is essential for further expansion.

## INTRODUCTION

The anodization of silver electrodes in alkaline solutions has been extensively investigated. Reviews on the subject are given in references[1–5]. The anodic reaction involves two oxidation levels corresponding to $Ag_2O$ and $AgO$ formation. The corresponding reactions were principally investigated at 298 K, although data down to 258 K[3] and up to 478 K has been reported[6, 7].

The first oxidation level comprises as a first step the formation of a AgOH monolayer[8–11] followed by thickening to produce a homogeneous Ag(I) oxide primary layer. A second Ag(I) oxide layer is formed through nucleation and 3-D growth under diffusion control of isolated Ag(I) oxide centers[12–15].

The second oxidation level of silver anodization corresponds to the formation of a Ag(II) oxide layer on top of the complex Ag(I) oxide layer[5]. Earlier kinetic studies of Ag(II) oxide formation[11, 16–19] were interpreted through different mechanisms, that is either a conventional heterogeneous electrochemical reaction mechanism, such as the autocatalytic mechanism[17] and the transfer of $O^{2-}$ ions at the $Ag_2O$–$AgO$ interface[16], or nucleation and growth rate controlling processes[5, 10, 11, 18, 19]. These models, however could not explain the marked decrease in the Ag(II) oxide charge with potential result-. ing from the crystal formation under a constant applied potential set in the 0.51–0.56 V range (*vs sce*). Nevertheless, despite these discrepancies it should be noticed that the kinetic interpretation based upon a progressive nucleation of AgO centers coupled with 3-D growth appears as the most satisfactory one[18]. It implies a mechanism of lattice formation based on the concentration and potential dependence of crystal growth.

The present paper refers to the electroformation of the Ag(II) oxide layer under potentiodynamic and potentiostatic conditions. Data are discussed in terms of both a nucleation and growth model which accounts for the entire current transient behaviour complemented with a statistical analysis of the induction times related to the nucleation kinetics of the Ag(II) oxide crystals.

## EXPERIMENTAL

Working electrodes were made of polycrystalline (pc) Ag (99.99% purity) rods axially embedded in Araldite cylindrical holders to obtain circular silver exposed areas of 0.05 cm² apparent area surrounded by an insulating ring of 0.6 cm outer dia. The electrodes were mechanically polished starting with fine grained emery paper and followed with alumina paste of 1 μm dia. to obtain mirror polished silver electrode surfaces. Before the electrochemical measurements the electrodes were degreased with alcohol and rinsed with triply distilled water. Precautions were taken to avoid crevices between Ag rods and Araldite holders which could lead to artifacts in the electrochemical measurements. The counter electrode was a large Pt sheet located in a separate cell compartment. The potential of the working electrode was measured against a saturated calomel electrode (*sce*) connected to the working electrode cell compartment through a Luggin–Haber capillary tip. Potentials in the text are referred to the *sce*. The electrolyte solution was 0.1 M NaOH prepared from triply distilled water and AR chemicals. Solutions were bubbled with purified nitrogen for 3 h prior to the electrochemical runs. The working electrode was subjected only to a single triangular potential scan between the cathodic ($E_{s,c}$) and the anodic ($E_{s,a}$) switching potentials. Repetitive potential scans were specifically avoided as the electroreduction of the silver oxide layer results in reformed[5] Ag surfaces made of a large number of overlapping nuclei with complex diffusional paths. For this reason a new fresh polished Ag electrode was required for each measurement. Current transients at constant potential were obtained in the conventional way by using the perturbing potential programs described in the text. In all these cases the Ag electrodes

were held at $E_{s,c} = -1.20$ V, for 60 s, to start every electrochemical run with a reproducible electroreduced silver electrode surface. All measurements were made at $T = 25\,°C$. Experiments were also made by using a working electrode consisting of a Ag(I) oxide layer chemically precipitated on the base of a spectroscopy grade graphite rod (0.28 cm²). The purpose of this electrode was to investigate the Ag(I) oxide→Ag(II) oxide reaction without the possible interference of base silver phase electrochemical reactions. The precipitation of the Ag(I) oxide was made by alternately dipping in 0.1 M AgNO₃ and 0.1 M NaOH solutions as indicated elsewhere[20].

## RESULTS

### *Voltammetric data*

The $j$–$E$ profile of a polycrystalline silver electrode immersed in 0.1 M NaOH run at $v = 0.5 \times 10^{-3}$ V s⁻¹ between $E_{s,c} = -0.2$ V and $E_{s,a} = 0.65$ V shows up in the positive potential going scan peaks A′₁ and A″₁ at 0.23 V and 0.28 V, respectively, followed by a current decay until the potential reaches 0.53 V (Fig. 1). By further increasing the potential just a few mV a sudden increase in current defining a very sharp peak (A₂) located at 0.55 V can be observed. The returning scan from 0.6 V downwards shows a broad peak (C₂) at 0.37 V and a sharp peak (C₁) at 0.10 V. Peaks A′₁ and A″₁ are related to the electroformation of the primary Ag(I) oxide layer and to the nucleation and 3-D growth of the secondary Ag(I) oxide layer, respectively. The electroreduction of the complex Ag(I) oxide layer occurs in the potential range of peak C₁ leading to a reformed silver surface composed by a large number of overlapped nuclei[5]. The processes involved in the electroformation of the Ag(I) oxide layer were already discussed elsewhere[12]. Likewise, peak A₂ is attributed to the electroformation of an Ag(II) oxide layer and peak C₂ is assigned to the electroreduction of the Ag(II) oxide layer to form Ag(I) oxide[5, 12].

The height of peak A₂ $(j_p)$ vs $v^{1/2}$ plot (Fig. 2) exhibit two linear portions with a crossing point at $v \cong 1$ mV s⁻¹. Similarly two linear relationships are observed by plotting the potential of peak A₂ $(E_p)$ vs log $v$ (Fig. 3) with the slopes 0.03 V dec⁻¹ and 0.09 V dec⁻¹, respectively. The charge density $(q_{A_2})$ obtained from peak A₂ decreases sharply as $v$ increases. Otherwise, $q_{C_2}$, the charge density derived from peak C₂, is considerably smaller than $q_{C_1}$, the charge density of peak C₁, the corresponding ratio being $(q_{C_2}/q_{C_1}) \cong 0.3$. To evaluate the contribution of the electrooxidation of Ag substrate and that of the Ag(I) oxide phases to the processes occurring at A₂, the voltammetric data derived from the Ag(I) oxide layer chemically deposited onto a graphite disc electrode becomes important. For this purpose the Ag(I) oxide electrode was polarized at 0.4 V, that is in the Ag₂O electroformation potential range (Fig. 1), and subsequently potential scanned up to 0.65 V and backwards to −0.2 V. The corresponding $j$–$E$ profile exhibits the same characteristics already depicted in Fig. 1 with nearly the same $q_{C_2}/q_{C_1}$ ratio. This fact is a clear indication that the process occurring in the
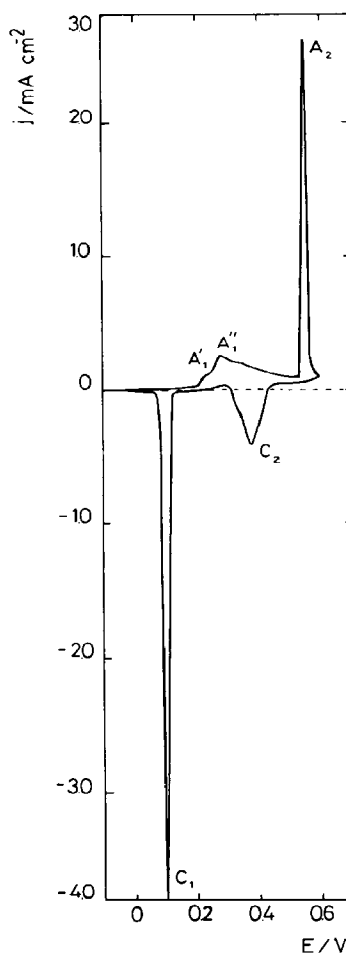


Fig. 1. Voltammogram for a polycrystalline Ag electrode run in 0.1 M NaOH at 25°C between $E_{s,c} = -0.2$ V and $E_{s,a} = 0.6$ V at $v = 0.5 \times 10^{-3}$ V s⁻¹.

potential range of peak A₂ involves only a partial conversion of the Ag(I) oxide into Ag(II) oxide. According to X-ray diffraction data the Ag(II) oxide layer is formed at the Ag₂O layer side in contact with the electrolyte[21].

### *Potentiostatic current transients*

Current transients run under a preset constant potential step $(E_s)$ were made after applying to the mechanically polished working electrode the following pretreatment. Firstly, the electrode was immersed in 0.1 M NaOH and the potential was held at $E_c = -1.20$ V for $t_c = 60$ s to obtain a reproducible electroreduced silver surface. Subsequently, the potential was stepped to $E_a = 0.45$ V for $t_a = 300$ s to attain a steady condition for the electroformation of the Ag(I) oxide layer. Changes in $t_a$ from 300 to 1200 s have no influence in the transient displays. Finally, the potential was stepped to $E_s$ ($0.5 \leq E_s \leq 0.6$ V) to record the
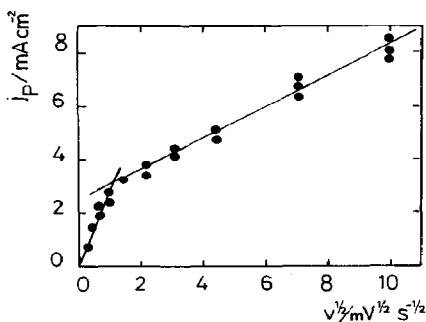
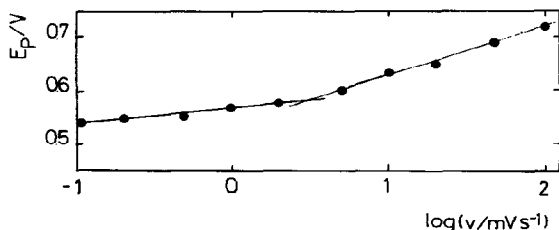Fig. 2. Peak current (A$_2$) $vs$ $v^{1/2}$ plot. 0.1 M NaOH, 25°C.



Fig. 3. $E_p$ (A$_2$) $vs$ log $v$ plot. 0.1 M NaOH, 25°C.

current transients related to the partial electrooxidation of the Ag(I) oxide layer into Ag(II) oxide.

The current transients exhibit the following features. Initially the current remains nearly constant (background current) for a certain time. This time can be considered as an induction time ($t_i$) related to the oxide conversion process (insert in Fig. 4). Later for $t_s > t_i$, the current increases to attain a maximum ($I_M$) at the time $t_M$, and finally for $t > t_M$ the current decreases markedly to approach the initial background current (Fig. 4). As $E_s$ shifts in the positive direction both $t_i$ and $t_M$ decrease and $I_M$ increases, but $q$, the charge density involved in the transients decreases sharply as $E_s$ increases (Fig. 5) in contrast to the expectations for a single layer nucleation and growth process[18]. The behaviour of these current

transients is similar to those described previously. This charge decrease can be related to the change in the multilayer structure of the anodic layer. As the $E_s$ is positively increased it appears as if a more compact outer AgO layer is produced, $ie$ the passive character of this layer increases, so that only a relatively smaller fraction of Ag$_2$O transforms into AgO. This decrease in the yield of Ag$_2$O to AgO reaction has been observed at low temperatures due to slow nucleation[3].

Relevant information about the growth mode of the Ag(II) oxide nuclei can also be derived from the analysis of the initial rising part of the current transients which in all cases fits $j$ $vs$ $t^3$ linear relationships (Fig. 6) which go through the origin of coordinates because the time scale was set for $t = t_i = 0$. Furthermore, linear log $j_M$ $vs$ $E_s$ and log $t_M$ $vs$ $E_s$ plots are also obtained, the slope of the former being close to 0.06 V dec$^{-1}$ (Figs 7 and 8).

The time dependence of $P_{n \geqslant 1}$, the probability for the formation of at least one nucleus, can be used to probe new aspects of the nucleation kinetics. For a Poisson distribution and a stationary nucleation rate, $\bar{t}_i$, the mean value of the induction time, is given by[22]:

$$\bar{t}_i = \frac{1}{\alpha N_0}, \qquad (1)$$

where $\alpha N_0$ is the nucleation rate, $\alpha$ is the nucleation rate constant and $N_0$ denotes the number of sites available for nucleation. To test Equation (1) a large number of $t_i$ were measured for each $E_s$ value so that $P_{n \geqslant 1}$ was obtained as a function of time. The $P_{n \geqslant 1}$ $vs$ $t$ plots (Fig. 9) indicate that as $E_s$ moves in the positive direction the survival time, i.e. the time for which the sample remains free of AgO nuclei, is drastically reduced.

## DISCUSSION

The present results can be directly discussed within the framework of certain controversial theories about the growth mode of the Ag(II) oxide centers during silver anodization at relatively high anodic potential in basic solutions, in particular the participation of a
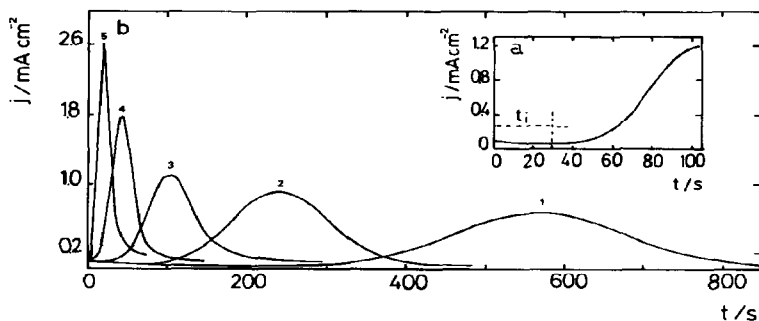


Fig. 4. Potentiostatic current transients of polycrystalline Ag electrode in 0.1 M NaOH after applying the following successive potential step pretreatment: $E_c = -1.20$ V; $t_c = 60$ s potential holding at $E_a = 0.45$ V for $t_a = 300$ s and potential stepped to $E_s$. (a) Initial portion of current transient and definition of $t_i$. (b) Current transients recorded at different $E_s$. (1) $E_s = 0.51$; (2) $E_s = 0.52$; (3) $E_s = 0.53$; (4) $E_s = 0.54$; (5) $E_s = 0.55$ V.
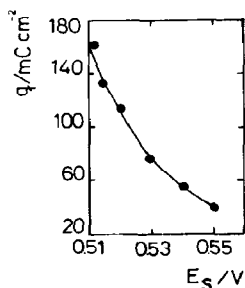
Fig. 5. Charge density resulting from current transient integration *vs* $E_s$. Data from Fig. 4b.
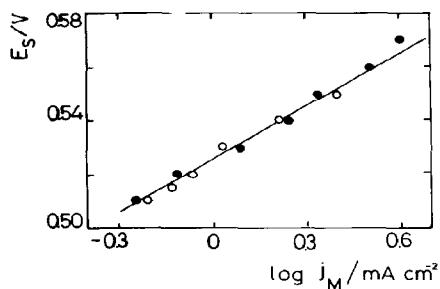


Fig. 7. Potential dependence of the current maxima resulting from the current transients. Polycrystalline Ag electrode in 0.1 M NaOH. Electrode treatment as described in Fig. 4b.
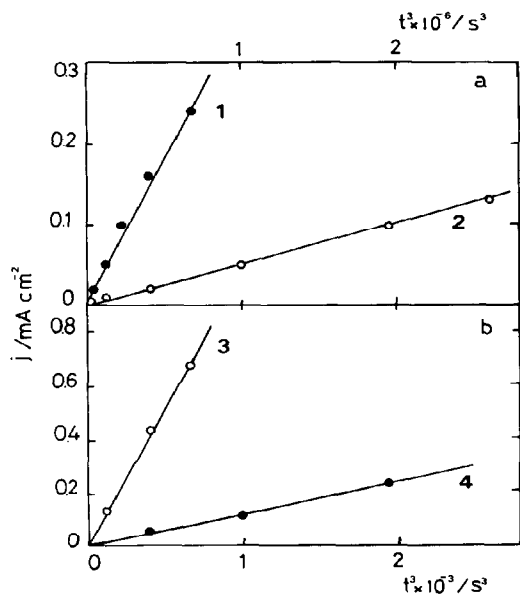


Fig. 6. *j vs* $t^3$ plots for the middle rising portions of the current transients depicted in Fig. 4b. (a) (1) $E_s = 0.52$; (2) $E_s = 0.51$ V. (b) (3) $E_s = 0.55$; (4) $E_s = 0.54$ V. Time scale origin is $t = t_i = 0$.
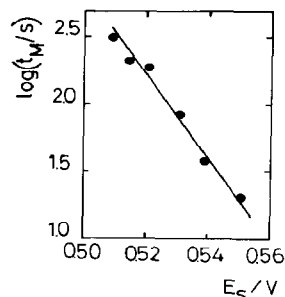


Fig. 8. Potential dependence of $t_M$.

nucleation stage in the Ag(I) oxide→Ag(II) oxide reaction. This reaction involves a phase change for which both a charge transfer and a diffusion controlled growth mechanism have been proposed, based on the analysis of the current transient data. In principle, one can admit that the strong dependence of $I_M$ and $t_M$ on $E_s$ favours a charge transfer controlled process, although simple 3-D growth models for this type of control predict that the current increases asymptotically to a limiting value when $t \rightarrow \infty$ instead of the maximum value resulting in the transients. On the other hand, it is clear from the voltammetric data that the behaviour of peak $A_2$ perhaps indicates the pres-
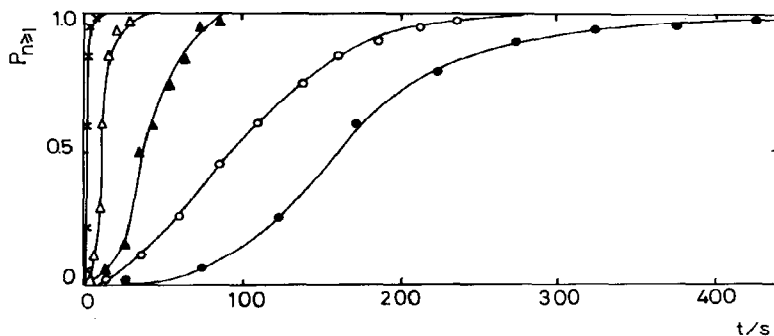


Fig. 9. Time dependence of $P_{n \geq 1}$ for various potential steps: (●) $E_s = 0.51$; (○) $E_s = 0.52$; (▲) $E_s = 0.53$; (△) $E_s = 0.54$; (×) $E_s = 0.56$ V.

ence of mass transport limitations (Fig. 2). Otherwise, it should be noticed that 3-D growth under diffusion control requires either $I$ $vs$ $t^{1/2}$ or $I$ $vs$ $t^{3/2}$ linear relationships for the initial rising part of the current transients and linear $I$ $vs$ $t^{-1/2}$ relationship for $t \to \infty$. However, the initial rising part of the transients actually fit linear $I$ $vs$ $t^3$ instead of $I$ $vs$ $t^{3/2}$ linear relationships (Fig. 6) and the portion of the transients after the maximum decays faster than that expected for a $I$ $vs$ $t^{-1/2}$ plot. Nevertheless, despite these drawbacks for the present system, the progressive nucleation and 3-D growth under charge transfer control where diffusion of species from the electrode to the growing sites is essential for further expansion seems to be applicable[23, 24]. For such a model the current–time transients for the case where pyramids are right circular cones is given by the following equations[23]:

$$j(t) = zFk_2\left[1.0 - \exp\left(-\frac{\pi M^2 k_1^2 \alpha N_0 t^3}{3\rho^2}\right)\right]$$

$$\exp\left(-\frac{\pi M^2 k_1^2 \alpha N_0 t^3}{3\rho^2}\right) \qquad (2)$$

$$= P_1[1.0 - \exp(-P_2 t^3)][\exp(-P_2 t^3)], \quad (3)$$

where $j(t)$ is the instantaneous current density, $P_1 = zFk_2$, $P_2 = \pi M^2 k_1^2 \alpha N_0/3\rho^2$, $M$ is the molecular weight and $\rho$ is the density of the electroformed deposit, $N_0$ is the number of sites available for nucleation, $\alpha$ is the nucleation rate constant, so that $\alpha N_0$ is the nucleation rate, and $k_2$ and $k_1$ are the specific rate constants for crystal growth perpendicular and parallel to the electrode surface, respectively. The final factor in Equations (2) and (3) accounts for the reduction of growth caused by the diffusion of species to the growth sites. It can be noticed that the decrease in $q$ as $E_s$ increases (Fig. 5) indicates that certain "passivation" of the electrode probably occurs through the formation of a more compact Ag(II) oxide layer at positive potentials which prevents the access of the

reactants to the Ag(I) oxide layer. From the $q$ $vs$ $E_s$ dependence (Fig. 5), the change in the average thickness of the AgO layer with $E_s$ can be estimated from:

$$h = \left(\frac{M}{zF\rho}\right)q. \qquad (4)$$

By taking $M_{Ag_2O_2} = 246 \text{ g mol}^{-1}$, $z = 2$, $\rho = 7.143 \text{ g cm}^{-3}$; $h$ becomes 2 and 0.4 $\mu$m for $E_s = 0.51$ and 0.55 V, respectively.

Equation (3) predicts a linear $I$ $vs$ $t^3$ plot for $t \to 0$, and linear log $I_M$ $vs$ $E_s$ and log $t_M$ $vs$ $E_s$ relationships which have been proved experimentally (Figs 7 and 8). Furthermore, a reduced variable test for different $E_s$ after $t_i$ and background current subtraction, shows an excellent agreement with the theoretical curve (Fig. 10). Unfortunately, information about the nucleation stage can not be obtained from the transients as $P_2$ contains the composite $k_1^2 \alpha N_0$ term, but it can be derived through the statistical analysis of $t_i$ and by using the $[1 - P_{n \geq 1}]$ $vs$ $t$ and ln $\lambda$ $vs$ $\eta$ plots, where $\lambda$ corresponds to an average nucleation rate derived from the plots shown in Figs 11 and 12. Therefore, on the basis of an irreversible electrochemical nucleation kinetic formalism[25], the value of the rate $\alpha N_0$ as derived from $\lambda/a$ ratio, $a$ being the electrode area, allows now the calculation of the rate constant $k_1$ from the value of $P_2$, and the rate constant $k_2$ directly from $P_1$. Both rate constants fit log $k_1$ and log $k_2$ $vs$ $\eta$ plots with slopes close to 0.06 V decade (Fig. 13) but at a fixed potential the value of $k_1$ is practically three orders of magnitude greater than that of $k_2$. This difference would explain the fact that under certain conditions the overall process would approach a 2-D growth model. Furthermore, it should be noticed that for a progressive nucleation and 2-D growth under charge transfer control $j(t)$ is given by[26]:

$$j(t) = \frac{zF\pi Mhk^2 N_0 \alpha}{\rho} t^2 \exp\left[-\frac{\pi M^2 k^2 N_0 \alpha}{3\rho^2} t^3\right] \qquad (5)$$
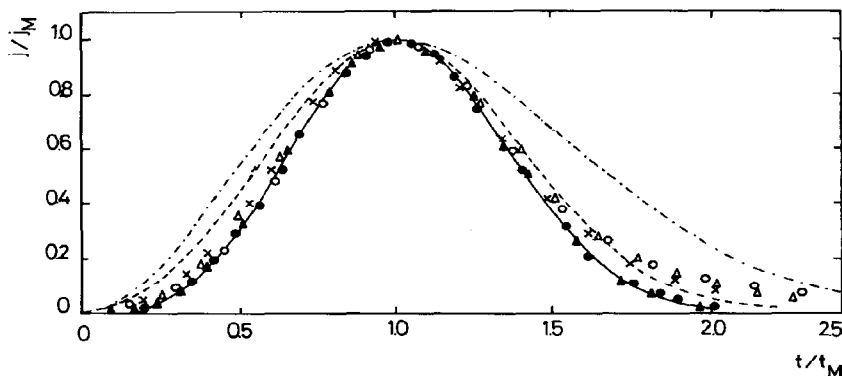
$$= P_3 t^2 \exp(-P_4 t^3) \qquad (6)$$

Fig. 10. Dimensionless [$I/I_M$ $vs$ $t/t_M$] plots for current transients depicted in Fig. 4b. (▲) $E_s = 0.51$ V; (●) $E_s$ = 0.52 V; (○) $E_s = 0.53$ V; (×) $E_s = 0.54$ V; (△) $E_s = 0.55$ V. Theoretical results from the models correspond to the three lines as follows. Progressive (———) and the instantaneous (–·–·) nucleation and 3-D growth under charge transfer control for right circular cones leading to passivation. Progressive (– – – –) nucleation and 2-D growth under charge transfer control for right cylinders growing radially.
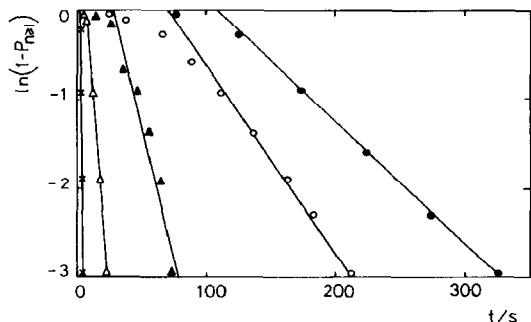
Fig. 11. ln $(1\text{-}P_{n \geqq 1})$ *vs* $t$ plots resulting for different values of $E_s$; (●) $E_s = 0.51$; (○) $E_s = 0.52$; (▲) $E_s = 0.53$; (Δ) $E_s = 0.54$; (×) $E_s = 0.56$ V.
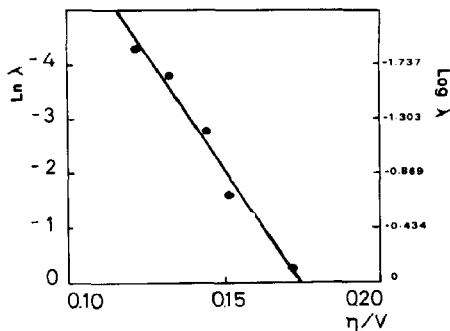


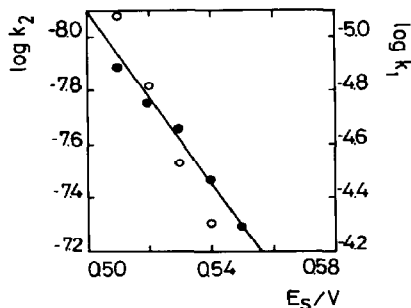Fig. 12. Overpotential dependence of the average steady state nucleation rate according to the atomistic model.
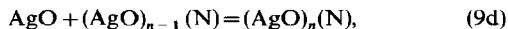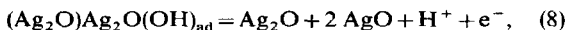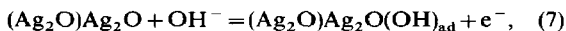


Fig. 13. Potential dependence of $k_1$ and $k_2$.

The reduced variable test for Equation (6) (Fig. 10) suggests that this model accounts for the transients behaviour for $t \rightarrow \infty$. Otherwise for $t \rightarrow 0$, the expected linear $I$ *vs* $t^2$ plots are not satisfactorily fulfilled in the short time range (Fig. 6). Therefore, from the entire kinetic analysis one can conclude that the progressive nucleation and 3-D growth model under charge transfer control followed by passivation becomes the most adequate to describe the present experimental results.

On the other hand, the following reaction sequence can account for the kinetics of the $Ag_2O \rightarrow AgO$ phase

change:

$$(Ag_2O)Ag_2O + OH^- = (Ag_2O)Ag_2O(OH)_{ad} + e^-, \quad (7)$$

$$(Ag_2O)Ag_2O(OH)_{ad} = Ag_2O + 2\ AgO + H^+ + e^-, \quad (8)$$

$$AgO + N = AgO(N), \quad (9a)$$

$$AgO + AgO(N) = (AgO)_2(N)^*, \quad (9b)$$

$$AgO + (AgO)_2(N) = (AgO)_3(N), \quad (9c)$$

$$AgO + (AgO)_{n-1}(N) = (AgO)_n(N), \quad (9d)$$

where N denotes a preferred site in the Ag(I) oxide layer where nucleation of the AgO species takes place, the asterisk denotes the critical nucleus. Equations (7) and (8) imply successive electron transfer steps and Equation (9a)–(9d) represent the nucleation and growth stage.

The physical picture of the postulated model means that when the applied potential exceeds the potential of the $Ag_2O/AgO$ redox couple $[E_r(10^{-1}M\ NaOH)/vs\ sce = 0.388]$ the outer part of the $Ag_2O$ layer is electro-oxidized yielding a critical supersaturation of AgO species. So that nuclei of AgO, probably dimers, are progressively formed and grow under charge transfer control, the mode of growth of nuclei approaching circular right cones.

On the other hand, at low $\eta$ values, that is for low supersaturations, isolated centres of Ag(II) oxides grow slowly, and under this condition the $OH^-$ ions can react easily with the remaining Ag(I) oxide crystals. Oppositely at high $\eta$ values, *ie* large supersaturations, a large number of centres grow rapidly yielding a compact Ag(II) oxide layer which prevents further reaction between the $OH^-$ ions and the Ag(I) oxide crystals. This explains the "passivation" of the Ag(I) oxide electrode as $\eta$ increases. It should also be noticed that in agreement with the advanced interpretation of the present results Monte Carlo simulations of crystal growth at low supersaturations indicate elongated shapes instead of the more compact cap-shaped crystallites formed at high supersaturations[27, 28].

## REFERENCES

1. L. Young, *Anodic Oxide Films*, p. 302, Academic Press, London (1961).
2. J. P. Hoare, *The Electrochemistry of Oxygen*, p. 211, Interscience, New York (1968).
3. B. V. Tilak, R. S. Perkins, H. A. Kozlowska and B. E. Conway, *Electrochim. Acta* **17**, 1447 (1972).
4. N. A. Shumilova and G. V. Zhutaeva, in *Encyclopedia of Electrochemistry of the Elements* (Edited by A. J. Bard), Vol. VIII, p. 1, Dekker, New York (1978).

5. J. M. M. Drogg and F. Huisman, *J. electroanal. Chem.* **115**, 211 (1980).
6. B. G. Pound, D. D. McDonald and J. W. Tomlinson, *Electrochim. Acta* **25**, 563 (1980).
7. B. G. Pound, D. D. MacDonald and J. W. Tomlinson, *Electrochim. Acta* **25**, 1293 (1980).
8. P. Stonehart, *Electrochim. Acta* **13**, 1789 (1968).
9. G. T. Burnstein and R. C. Newman, *Electrochim. Acta* **25**, 1009 (1980).
10. M. López Teijelo, J. R. Vilche and A. J. Arvia, *J. electroanal. Chem.* **131**, 331 (1982).
11. I. Dugdale, M. Fleischmann and W. F. K. Wynne-Jones, *Electrochim. Acta* **5**, 229 (1961).
12. M. Fleischmann, D. J. Lax and H. R. Thirsk, *Trans. Faraday Soc.* **64**, 3128 (1968).
13. J. M. M. Drogg, P. T. Arderliesten and G. A. Bootsma, *J. electroanal. Chem.* **99**, 173 (1979).
14. G. W. D. Briggs, M. Fleischmann, D. J. Lax and H. R. Thirsk, *Trans. Faraday Soc.* **64**, 3120 (1968).
15. J. Gomez Becerra, R. C. Salvarezza and A. J. Arvia, *Electrochim. Acta* **33**, 1431 (1988).
16. R. G. Barradas and G. H. Fraser, *Can. J. Chem.* **42**, 2488 (1964).
17. P. Stonehart and F. P. Portante, *Electrochim. Acta* **13**, 1805 (1968).
18. M. Fleischmann, D. J. Lax and H. R. Thirsk, *Trans. Faraday Soc.* **64**, 3137 (1968).
19. R. S. Perkins, B. V. Tilak, B. E. Conway and H. A. Kozlowska, *Electrochim. Acta* **17**, 1471 (1972).
20. M. López Teijelo, J. R. Vilche and A. J. Arvia, *J. appl. Electrochem.* in press.
21. C. P. Wales and J. Burbank, *J. electrochem. Soc.* **106**, 855 (1959).
22. A. Milchev and V. Tsakova, *Electrochim. Acta* **30**, 133 (1985).
23. R. D. Armstrong, M. Fleischmann and H. R. Thirsk, *J. electroanal. Chem.* **11**, 208 (1966).
24. R. G. Barradas, P. C. Benson, S. Fletcher and J. D. Porter, *J. electroanal. Chem.* **85**, 57 (1977).
25. S. Fletcher, *J. electroanal. Chem.* **215**, 1 (1986).
26. M. Fleischmann and H. R. Thirsk, *Advances in Electrochemistry and Electrochemical Engineering* (Edited by P. Delahay), Vol. 3, p. 123, Wiley New York (1963).
27. D. Kashchiev, *J. Crystal Growth* **40**, 29, 47 (1977).
28. D. Kashchiev, *J. Crystal Growth* **67**, 559 (1984).